Model-Based Tracking for Autonomous Arrays

Michael B. Porter, Paul Hursky, Christopher O. Tiemann
Science Applications International Corporation
1299 Prospect St, Suite 305
La Jolla, CA 92037

Mark Stevenson
SPAWAR Systems Center, San Diego, CA 92152

Abstract- Over the last 30 years, model-based approaches to array signal processing have evolved considerably to the point where initial skepticism has been replaced by casual acceptance. Still challenges remain. In this work we are progressing to a fully autonomous implementation in which all of the processing is done within the array. Target tracks are then passed to the surface using acoustic links. This requirement is a big challenge in that the algorithms must be fast to operate in real-time on modest embedded computers. They also must be robust enough to function without human invention. We describe here one approach and its performance in an experimental sea test with a prototype autonomous array.

I. INTRODUCTION

In recent years, new acoustic sensors have been developed that are lightweight and use extremely low power. At the same time, inexpensive high-performance and low-power computers have become available. As a result a new generation of acoustic arrays has become practical that are easily deployed and perform all processing autonomously. A key challenge is to develop signal-processing algorithms with the usual desirable (but conflicting) characteristics of high probability of detection and low probability of false alarm. Since conventional plane-wave beamforming provides no ability to distinguish surface and submerged targets, model-based approaches are the likely answer. The acoustic model, of course, predicts the multipath structure, which in turn provides a unique signature of the source position in range, depth, and (often) azimuth.

A Venn diagram (Fig. 1) of alternatives for model-based localization would include 1) matched-field processing [1-4], 2) time-reversal/back-propagation [5-8], and 3) correlation methods [9-11]. These approaches all go back to the 1970's and though they sound quite different do indeed have a region of overlap in which the final algorithm is identical. This is important to remember since being aware of this overlap eliminates superficial claims about the benefits in terms of speed or robustness of one approach over the other. On the other hand, the different approaches begin from quite different perspectives and often suggest new directions or extensions that either would not be natural from another starting point or would not even be possible.

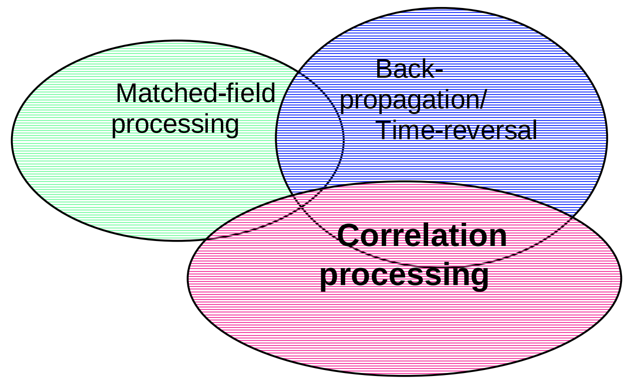

Fig. 1. Relationship between the various model-based processing schemes.

Our focus here is on the use of correlation approaches. To examine their performance, we conducted an experiment using a prototype autonomous array called Hydra (Fig. 2). This is a 6-phone sparse horizontal line array designed for autonomous operation (although for research purposes we are currently processing the data off line). The data from the Hydra Sea Test was recorded as an acoustic source was towed across the array.

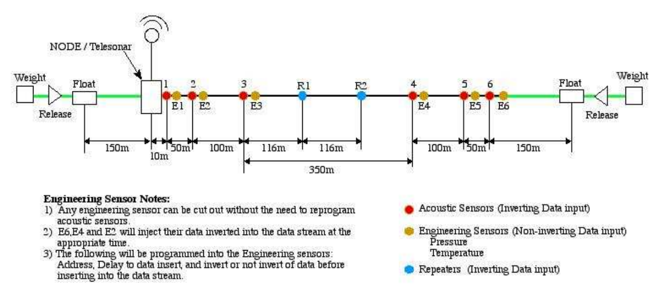

Fig. 2. Configuration of the Hydra array.

We process the data in two fashions. The first approach uses replica correlation in which a copy of the transmitted waveform is correlated with the received data. This case of a *known* source waveform is relevant for tracking AUV's or for the active scenario. The second approach uses auto- and cross-correlation of phone data and is relevant to the case of an *unknown* broadband source waveform. A pre-whitening stage is needed for signals with a strongly colored spectrum and this is done with a SCOT (smoothed coherence transform).

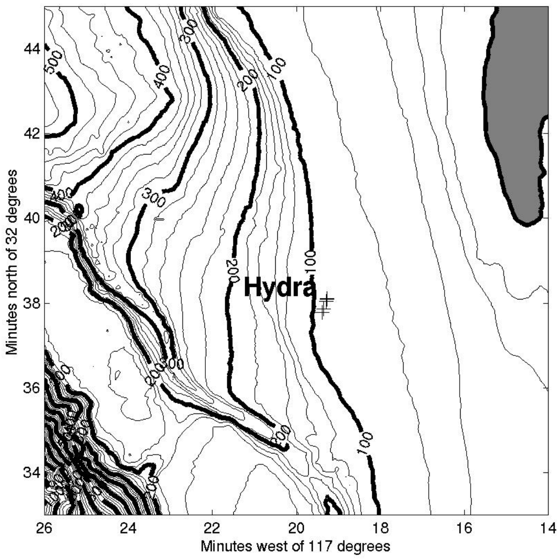

Fig. 3. Bathymetry in the vicinity of the Hydra array.

In either case, the received data shows a pattern of echoes (representing the channel impulse response or its auto/cross correlation). This pattern is a fingerprint of the source position so that the source is uniquely identified by comparison to an ensemble of predicted echo patterns that are generated by an acoustic model. This paper will both demonstrate the processing and discuss the pros and cons of several variants.

II. EXPERIMENTAL SCENARIO

The Hydra array was deployed on the seafloor in an area off the coast of California near San Diego on July 26, 2000 as shown in Fig. 3. The water depth at the array was about 100 m, varying by some 15 m over the area of the source tows.

Geo-acoustic data for the site are well known from previous studies in the area. The ocean sound speed profile was measured during the experiment and showed a downward refracting shape shown in Fig. 4. A sense of the propagation conditions is given by a TL plot and ray trace shown in Fig. 5 for a source depth of 30 m.

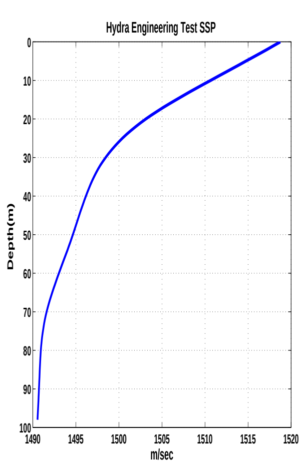

Fig. 4. Sound-speed profile measured during the Hydra Sea Test.

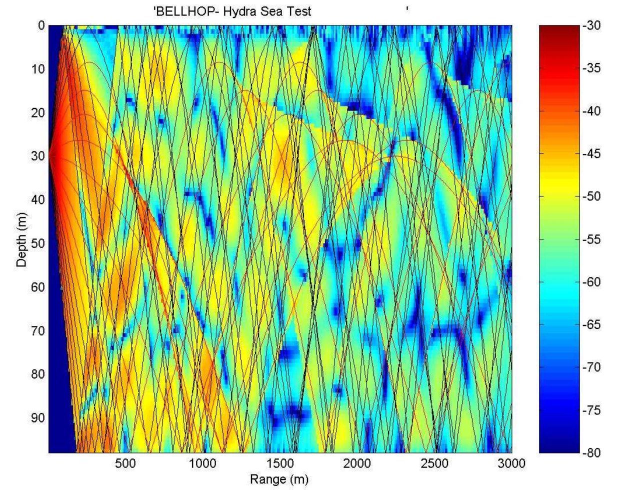

Fig. 5. Ray-trace superimposed on transmission loss for the test site.

III. ACOUSTIC TRANSMISSIONS

Sources of interest for this array include both marine mammals and surface ships. To provide a waveform with characteristics representative of such sources, both tonals and LFM chirps were transmitted. The chirps swept from 30-330 Hz over a 3-second interval and were repeated every 6 seconds. A plot of the spectrogram (Fig. 6) on one of the phones shows the typical 'bathtub pattern' as the source passed through the closest point of approach (CPA). The nearly vertical striations are the LFM chirps and the horizontal striations are the tonals.

A. Replica Correlogram

We next correlate the received waveform with a replica of the source waveform:

$$rr(t) = \int r(\tau - t)s(\tau)d\tau \,. \quad (1)$$

The resulting function, $rr(t)$, is referred to as the replica-correlogram or matched-filter output. This is a fairly standard procedure but we will review it briefly.

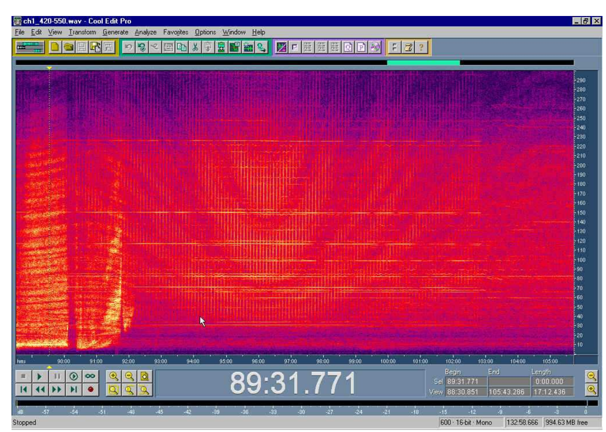

Fig. 6. Spectrogram of one of the Hydra channels during an overpass by the tow ship.

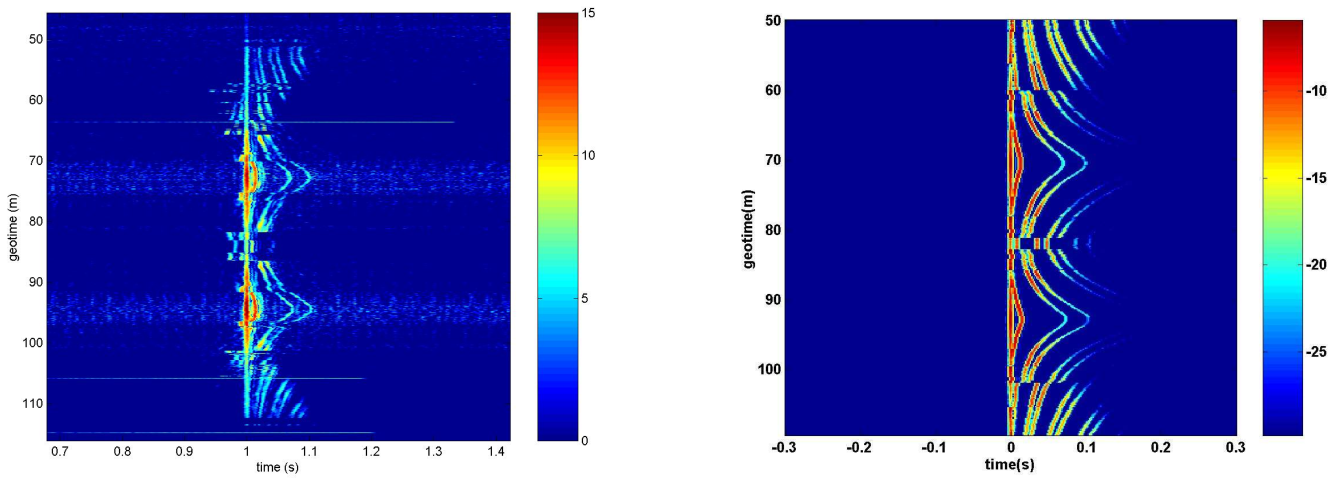

Fig. 7. Measured (left) and modeled (right) channel impulse response as the source is towed over the array and back again

The received waveform is a sum of delayed and scaled versions of the source waveform:

$$r(t) = \sum A_i s(t - t_i)\,. \qquad (2)$$

More generally, we also obtain additional terms involving the Hilbert transform of the waveform. The combination of the waveform and its Hilbert transform represents all possible phase changes. However, for simplicity we neglect these effects.

Replica correlation then yields

$$rr(t) = \int \sum A_i s(\tau - t + t_i) s(\tau) d\tau = \sum A_i ss(t - t_i)\,, \qquad (3)$$

where, $ss(t)$, is the auto-correlation function of the source:

$$ss(t) = \int s(\tau - t) s(\tau) d\tau\,. \qquad (4)$$

Thus if we make $ss(t)$ a sharp function like the delta-function we receive a pattern of impulses with peaks matching the strengths and delays of the echoes in the channel; in mathematical terms it approximates the Green's function. The autocorrelation of an LFM chirp is a sinc function and thus produces the desired impulse. The resulting replica-correlogram is shown in Fig. 7 with the wavefronts lined up by a 'leading edge', defined based on a threshold relative to the peak energy level. (The precise definition is important for the graphics but irrelevant for the source tracking described later.)

It is clear from the replica correlogram that the pattern of impulses received varies systematically with source position. However, to exploit this for localization, we either need to measure or model that dependence. Here we take the latter approach using the BELLHOP beam-tracing model to simulate the experimental scenario. The result shown in Fig. 8 shows a clear correspondence with the measured data, providing confidence in the simulation.

III. CORRELATION TRACKING WITH A KNOWN SOURCE SPECTRUM

We invert for the source position by comparing the measured impulse-response, $rr(t)$, to an ensemble of modeled versions, $hh(t;r_s,z_s)$, seeking the source coordinate, (r_s,z_s) that gives the best match between model and data. The comparison between model and data is done by a correlation:

$$C(r_s,z_s) = \max_t \int rr(t-\tau) hh(\tau;r_s,z_s) d\tau\,. \qquad (5)$$

This correlation $C(t;r_s,z_s)$, also depends on time in that it is built up as each new snapshot is processed. The resulting 3D function contains a snaking curve whose trajectory traces out the source motion in time and space. Slicing that ambiguity function at the true source depth of 30 m yields the range-time track shown on the left in Fig. 8. Similarly a slice in depth reveals the depth-time track shown on the right in Fig. 8. Both results agree well with the independent measures (GPS) taken during the experiment.

These results provide an effective demonstration of the algorithm; however, a further improvement can be obtained by processing all the phones in the array. This provides several benefits. First, the added information reduces ambiguities by introducing independent constraints. Second, it provides increased gain against noise. Third, it allows resolution in the azimuthal direction. The algorithm is a straightforward generalization in which additional auto-correlations are summed together to obtain the final ambiguity function. The effect is shown in Fig. 9 with the Hydra phone positions indicated by the '+' symbols. Note the left-right ambiguity, which is difficult to resolve with a nearly linear array.

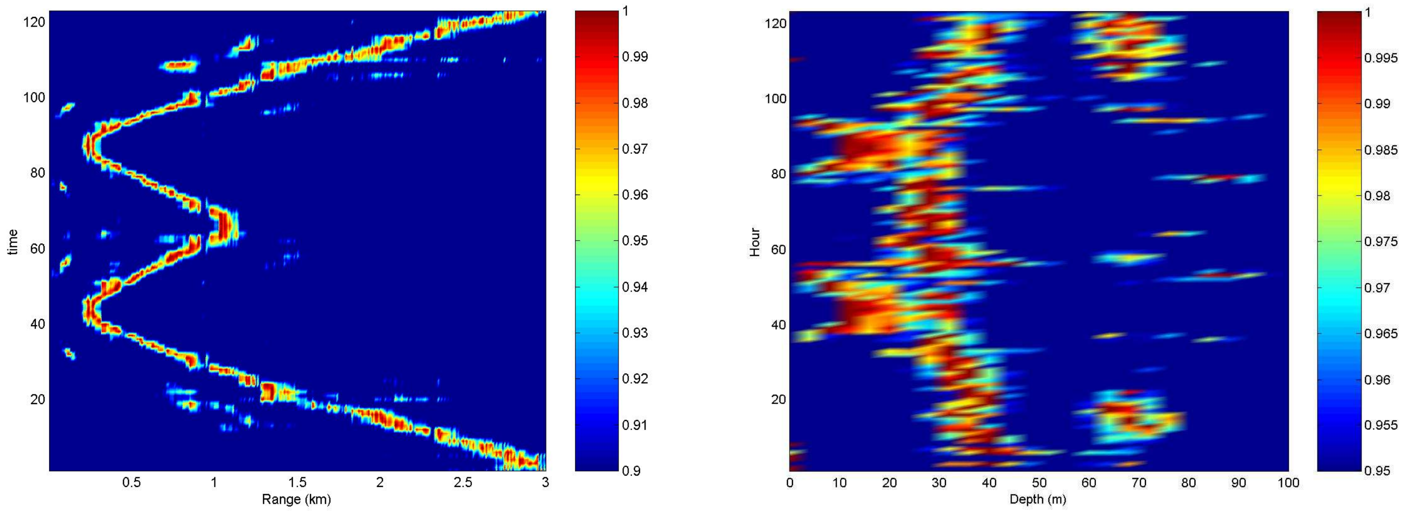

Fig. 8. Range-time (left) and depth-time track derived by correlation processing on a single phone.

IV. CORRELATION-TRACKING IN THE CASE OF UNKNOWN SOURCE SPECTRUM

The algorithm described above exploited knowledge of the source spectrum. It should be noted that there are important cases where this spectral information is available. However, when it is not the replica correlation is replaced by auto and cross-correlation.

To explain this process in more detail, consider first the auto-correlation processor. If the transmitted waveform has spectrum, $S(\omega)$, and the channel transfer function is $H(\omega)$ then the received spectrum is $R(\omega) = H(\omega)S(\omega)$. Therefore, the auto-correlation of the received waveform is $|H(\omega)|^2|S(\omega)|^2$. This is just the power spectrum of the channel and source spectra. The first may be also be interpreted as the auto-correlation of the channel impulse response. Similarly the second is the auto-correlation of the source waveform. Acoustic models predict $H(\omega)$ for candidate source positions. Thus, if we can filter the received time series in such a way as to remove the effects of the source spectrum, we can localize the source by comparing an ensemble of predicted channel auto-correlations to the measured one.

In many cases the source spectrum is white in the pass band of the array. In such cases the entire term associated with the source is unity and no further processing is required. However, when the source spectrum is colored or includes tonals the signal must be pre-whitened in some way. This is not as simple as it might first appear since the pre-whitening should eliminate ripples in the source spectrum while preserving ripples in the channel transfer function (since the latter are induced by the multipath structure and provide key information for source localization).

One standard pre-whitening approach is called the smoothed coherence transform or SCOT. In fact this is nothing more than a pre-whitening based on an averaged power level. The averaging time should be taken long enough to average out ripples in the channel transfer function. The process is illustrated in Fig. 10. The left panel is just a blow-up of the spectrogram shown previously in Fig. 6 showing more clearly the narrowband tonals superimposed on a broadband background. As mentioned above, the narrowband tonals were part of the transmitted waveform and represented about 50% of the total source energy. Since the autocorrelation of a tonal is a sinusoidal function of lag, the tonal would overwhelm the results and prevent us from localizing the source.

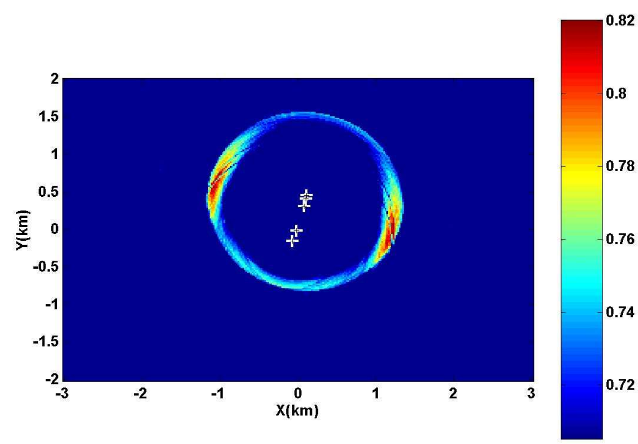

Fig. 9. Range/cross-range snapshot generated by correlation processing of multiple phones.

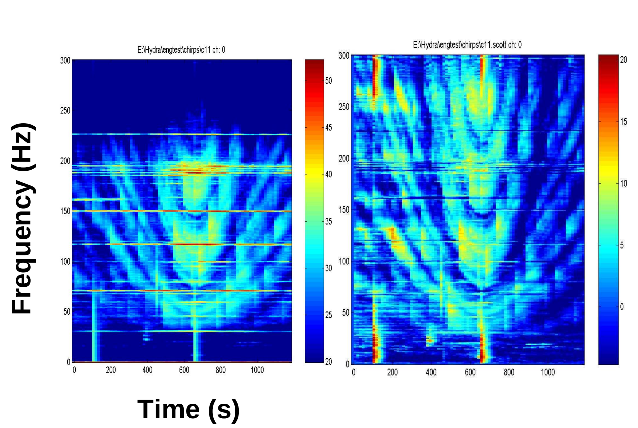

Fig. 10. Spectrogram for a single phone as the source passed over the Hydra array before (left) and after (right) pre-whitening.

To summarize the procedure for unknown source spectrum: we prewhiten and form both auto- and cross-correlation time series for all possible phone combinations. As each channel receives multiple echoes of the source time series, we get a sequence of spikes as echoes in one channel line up in time with other echoes in the other channel. Just as in the replica correlation process, we then predict what this pattern should look like for an ensemble of hypothesized source positions. The ensemble of modeled patterns is then compared to the measured one and the 'similarity' (measured by correlation) is plotted as a function of hypothesized source position.

To understand how this works, it is useful to examine the auto- and cross-correlation plots during a period where the source passed over the array. The pair of plots in Fig. 11 is derived using an autocorrelation of a single phone using modeled (left) and measured (right) time series. Note again the systematic variation of the peaks as the source passes over the array. As discussed above, these peaks occur when one echo in the received data lines up with another. Naturally, there is always a peak in the auto-correlation function at zero lag. Figure 12 presents a similar comparison for cross-correlation of two different channels in the Hydra array. Note the agreement between the measured and simulated correlograms.

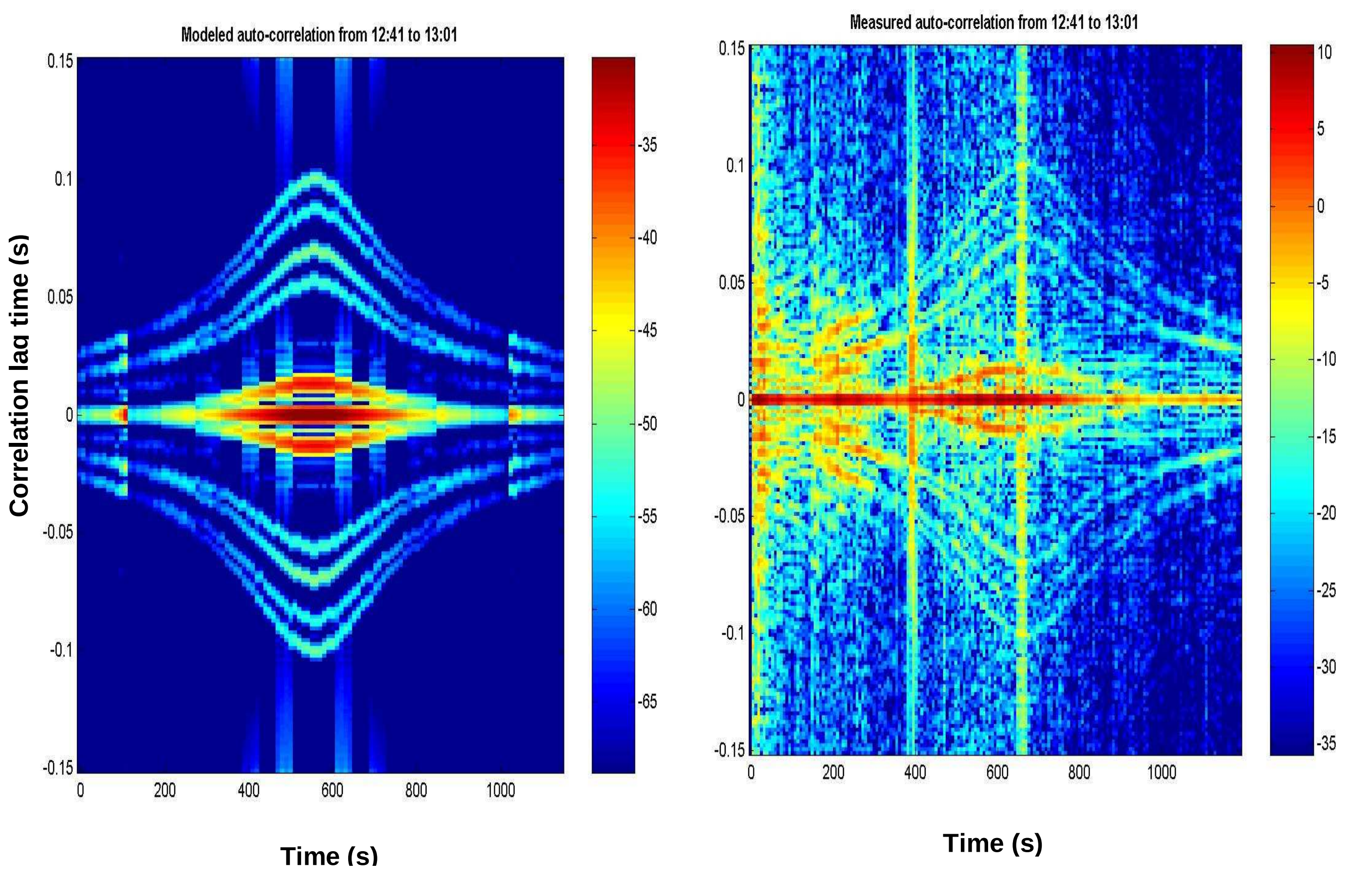

Fig. 11. Comparison of modeled (left) and measured (right) auto-correlations.

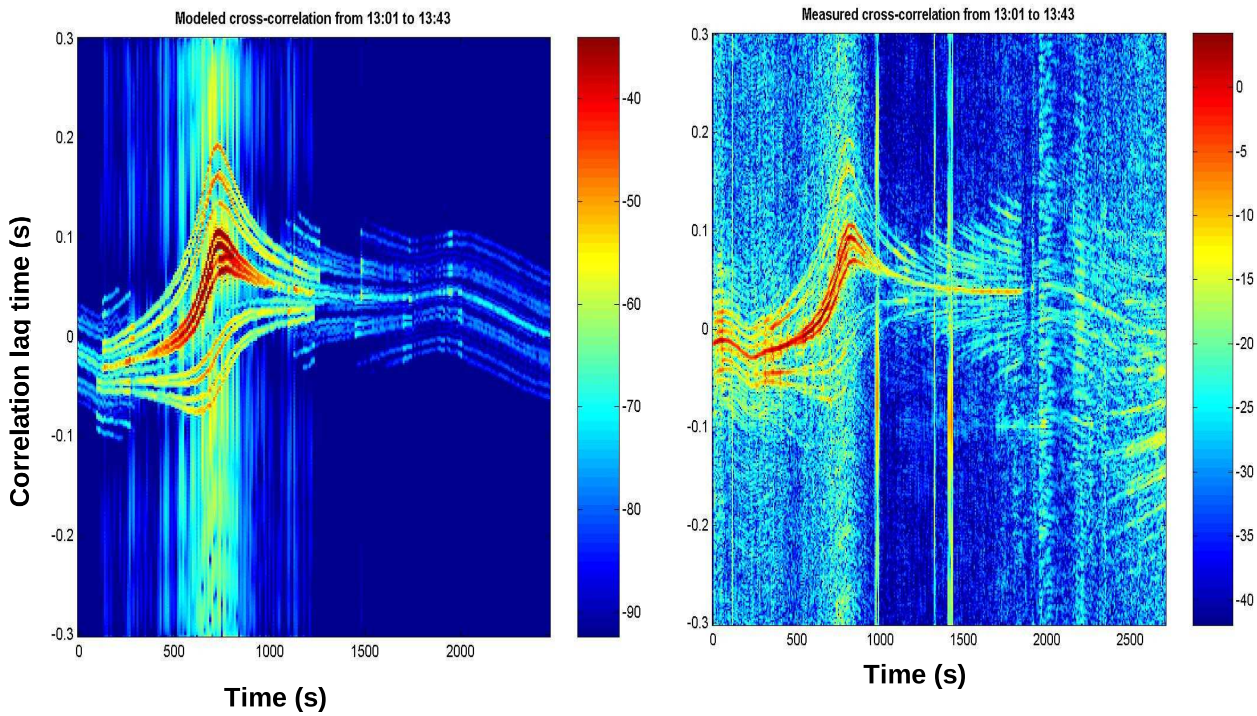

Fig. 12. Comparison of modeled (left) and measured (right) cross-correlations.

The final localization process can be done using every possible set of pair-wise correlations or using just subsets (even a single phone auto-correlation is sufficient for localization). The sequence of subplots in Fig. 13 shows some of the various options including replica correlation, auto-correlation, cross-correlation, and auto- and cross-correlation.

It is interesting to note how the auto and cross correlation results complement each other. The auto-correlation (and the replica correlation) produces an intersection of circles, so the ambiguity surface shows sidelobes that are normal to the radial from the array to the source. The cross-correlation produces an intersection of hyperbolae, so the ambiguity surface shows sidelobes along the asymptotes of the hyperbolae that are parallel to the radial from the array to the source. Combining these two results produces a locus of points that is the intersection of two perpendicular lines. The result is a very compact main peak in the composite ambiguity surface.

While these results provide some rough indication of the performance of the different options, it is worth noting that they do not provide a statistical measure. Similarly, the color scale used for plotting the results is essentially irrelevant and can be scaled arbitrarily. The important statistic is not the peak to sidelobe level on a single snapshot, but 'time-held', i.e. the percentage of time the peak is in the 'correct' position.

V. SUMMARY

Using the correlation-processing framework, we have demonstrated successful model-based localization using a prototype lightweight deployable array. Perhaps of greatest interest is the capability for depth discrimination, which is otherwise very difficult to automate. Future work will quantify the performance vis-à-vis matched-field processing and as a function of source level.

ACKNOWLEDGMENTS

This work was sponsored by ONR 321SS. Additional support was provided by ONR 321OA. We thank V. McDonald, M. Klausen, and J. Olson at SPAWARSSC for development work on the Hydra array. Finally, we benefited from numerous conversations with Phil Schey (SPAWARSSC) based on his own matched-field processing work with this data.

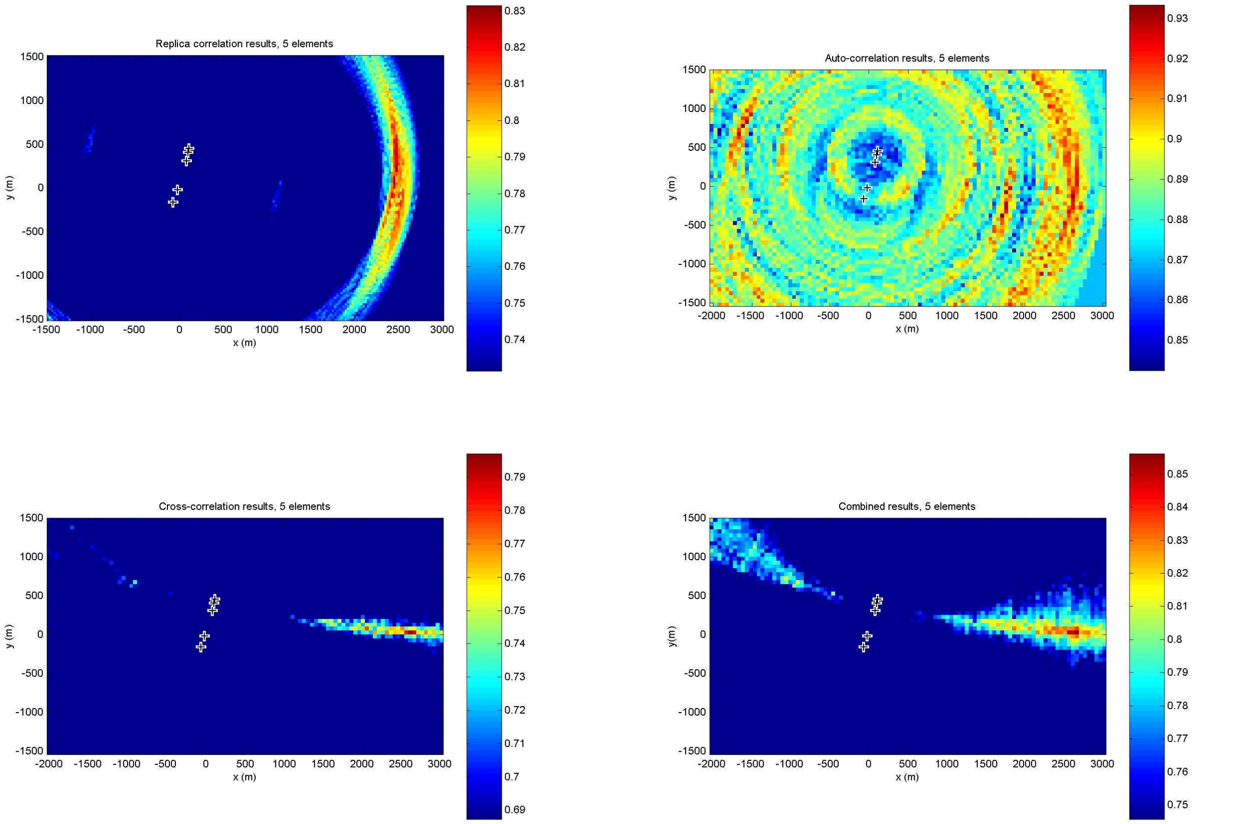

Fig. 13. Ambiguity surfaces generated via a) Replica correlation, b) Auto-correlation, c) Cross-correlation, and d) Auto- and cross-correlation.

REFERENCES

[1] H. P. Bucker, "Use of calculated sound fields and matched-field detection to locate sound sources in shallow water," *J. Acoust. Soc. Am.*, **59**,368-373 (1976).

[2] A.B. Baggeroer, W.A. Kuperman, P.N. Mikhalevsky, "An overview of matched-field methods in ocean acoustics", *IEEE J. Oceanic Eng.* **OE-18**(4):401-424 (1993).

[3] J.P. Ianniello, "Recent developments in SONAR signal processing", *IEEE Signal Processing Magazine*, **15**(4):27-40 (1998).

[4] A. Tolstoy, *Matched-Field Processing for Underwater Acoustics*, World Scientific, Singapore (1993).

[5] L. Nghiem-Phu, F. D. Tappert, and S. C. Daubin, "Source localization by CW acoustic retrogration," *Proceedings of a Workshop on Acoustic Source Localization*, internal NRL report, ed: R. Fizell, (1985).

[6] A. Parvulescu, ``Signal detection in a multipath medium by M.E.S.S. processing," *J. Acoust. Soc. Am.*, **33**, 1674- (1961).

[7] C. S. Clay, ``Waveguides, arrays and filters," *Geophysics*, **31**, 501-506 (1966).

[8] Michael B. Porter, "Acoustic Models and Sonar Systems," *IEEE J. of Oceanic Engineering*, Vol. OE-18(4):425–437 (1994).

[9] Jerome C. Rosenberger, "Passive Localization", *NATO ASI on Underwater Acoustic Data Processing*, ed. Y.T. Chan, pp. 511-524 Kluwer Press, Boston (1988).

[10] William S. Burdic, *Underwater Acoustic System Analysis*, 438-441, Prentice Hall, Englewood Cliffs (1991).

[11] M. Porter, S. Jesus, Y. Stéphan and X. Démoulin, E. Coelho, "Exploiting reliable features of the ocean channel response", *Shallow Water Acoustics*, R. Zhang and J. Zhou, Eds., China Ocean Press, p. 77-82, Beijing, China (1998).

[12] R.K. Brienzo and W.S. Hodgkiss, "Broadband matched-field processing", *J. Acoust. Soc. Amer.*, **94**(5), 2821-2831 (1993).

[13] Evan K. Westwood, "Broadband matched-field source localization", *J. Acoust. Soc. Amer.*, **91**(5):2777-2789 (1992).

[14] Evan K. Westwood and David P. Knobles, "Source track localization via multipath correlation matching", *J. Acoust. Soc. Amer.*, **102**(5), 2645-54 (1997).

[15] M. Porter, S. Jesus, Y. Stéphan, X. Démoulin, E. Coelho, "Tidal effects on source inversion", *Experimental Acoustic Inversion Methods*, Eds. A. Caiti, S. Jesus, J-P. Hermand, M.B. Porter, pp. 107-124, Kluwer (2000).

[16] Z.H. Michalopoulou, M.B. Porter, and J. Ianniello, "Broadband source localization in the Gulf of Mexico", *Journal of Computational Acoustics*, **2**(3),361–370 (1996).

[17] Newell O. Booth, Paul A. Baxley, Joseph A. Rice, Phil W. Schey, Willaims S. Hodgkiss, Gerald L. D'Spain, and James Murray, "Source localization with broad-band matched-field processing in shallow water", *IEEE J. Oceanic Eng.*, **21**(4), 402-412 (1996).

[18] C.S. Clay, "Optimum time-domain signal transmission and source location in a waveguide", *J. Acoustic. Soc. Amer.*, **81**(3):660-664 (1987).

[19] S.M. Jesus, "Broadband matched-field processing of transient signals in shallow water", *J. Acoust. Soc. Amer.*, **93**(4):1841-1850 (1993).

[20] L.N. Frazer and P.I. Pecholcs, "Single-hydrophone localization", *J. Acoust. Soc. Amer.*, **88**, 995-1002 (1990).

[21] F. Jensen, W. Kuperman, M. Porter and H. Schmidt, *Computational Ocean Acoustics*, Springer-Verlag, (2000).

[22] M. B. Porter, *The KRAKEN normal mode program*, SACLANT Undersea Research Centre Memorandum (SM-245) / Naval Research Laboratory Mem. Rep. 6920 (1991).